Computational Anthropomorphic Models of the Human Anatomy: The Path to Realistic Monte Carlo Modeling in Radiological Sciences

Habib Zaidi[1] and Xie George Xu[2]

[1]Division of Nuclear Medicine, Geneva University Hospital, CH-1211 Geneva 4, Switzerland; email: habib.zaidi@hcuge.ch

[2]Nuclear Engineering and Biomedical Engineering Programs, Rensselaer Polytechnic Institute, Troy, New York 12180; email: xug2@rpi.edu

Annu. Rev. Biomed. Eng. 2007. 9:471–500

First published online as a Review in Advance on February 13, 2007

The *Annual Review of Biomedical Engineering* is online at bioeng.annualreviews.org

This article's doi:
10.1146/annurev.bioeng.9.060906.151934

Copyright © 2007 by Annual Reviews.
All rights reserved

1523-9829/07/0815-0471$20.00

Key Words

anthropomorphic phantoms, stylized models, voxel-based models, Monte Carlo simulation, radiological imaging, dosimetry

Abstract

The widespread availability of high-performance computing and popularity of simulations stimulated the development of computational anthropomorphic models of the human anatomy for medical imaging modalities and dosimetry calculations. The widespread interest in molecular imaging spurred the development of more realistic three- to five-dimensional computational models based on the actual anatomy and physiology of individual humans and small animals. These can be defined by either mathematical (analytical) functions or digital (voxel-based) volume arrays (or a combination of both), thus allowing the simulation of medical imaging data that are ever closer to actual patient data. The paradigm shift away from the stylized human models is imminent with the development of more than 30 voxel-based tomographic models in recent years based on anatomical medical images. We review the fundamental and technical challenges of designing computational models of the human anatomy, and focus particularly on the latest developments and future directions of their application in the simulation of radiological imaging systems and dosimetry calculations.

Contents

INTRODUCTION

One of the most active areas of research and development in radiological sciences has been the advanced methods for calculating organ doses using computational models (phantoms) that represent the human anatomy. Such computational models are used extensively to derive many of the existing conversion parameters in radiation protection and nuclear medicine dosimetry, and to develop new image-reconstruction and processing algorithms in biomedical imaging (1). The prevalent accessibility of high-performance computing platforms, including multimode computer clusters and Grid technology, and popularity of simulations stimulated further the development of computational anthropomorphic models of the human anatomy. Such models are intimately tied to radiation transport simulation tools and modeling of diverse medical imaging modalities including single-photon emission computed tomography (SPECT), positron emission tomography (PET), X-ray computed tomography (CT), and magnetic resonance imaging (MRI).

Conceptually, the purpose of a physical phantom or computerized model is to represent an organ or body region of interest, to allow, for example (in nuclear medicine dosimetry), an understanding of how radiation emitted by a particular radiotracer distributed in various organs deposits energy in different tissues through various mechanisms of radiation interaction with matter (2). Such an understanding relies on assumptions about the chemical composition of the scattering medium, which determines the radiation transport processes that can be simulated using Monte Carlo methods. However, the physical phantoms, although experimentally important in benchmarking the data, are considered expensive, time-consuming, and sometimes unsafe to use, especially for large-scale operations. This review focuses on

computerized models that are advancing rapidly with the advent of increased computing power and multimodality medical imaging technologies. In other terms, a computerized model is a mathematical representation of an organ or tissue of the body, an organ system, or the whole body to allow accurate simulation of radiation transport and energy deposition using Monte Carlo methods.

Computerized anthropomorphic models can be defined by either equation-based (stylized) mathematical functions, digital (voxel-based) volume arrays, or hybrid equation-voxel models that mathematically describe organ boundaries from definitions extracted from voxel data. Stylized models consist of regularly shaped continuous objects defined by combinations of simple surface equations (e.g., right circular cylinders, spheres, or disks), whereas voxel-based models are derived mainly from segmented and labeled voxels from tomographic images of the human anatomy obtained from live subjects or cadavers by one of the available anatomical medical imaging modalities. Any complex radioactivity distribution and corresponding attenuation properties of the human body can therefore be modeled for any geometrical shapes. Stylized models, however, are more suitable for applications involving anatomical variability and temporal changes such as respiratory or cardiac motions. In addition, the disadvantage of the voxel-based approach is that inherent errors are introduced owing to the geometry voxelization. The discretization errors inherent in the voxelized representation may be reduced by finer sampling of the discretized data. More refined analysis of the advantages and drawbacks of stylized versus voxelized model representation for simulation of imaging systems has been described in the literature and will not be covered here (3, 4).

As a consequence of this generalized use, many questions are being raised, primarily about the need for and potential of human-body models, but also about how accurate they really are, how close to patient anatomy the anthropomorphic models used are, and what it would take to apply them clinically and make them widely available to the radiological imaging community at large. Many of these questions will be answered when patient modeling techniques are implemented and used for more routine calculations and for in-depth investigations. This review summarizes the latest efforts and future directions in the development of computational anthropomorphic models for application in radiological sciences. Although historically the term phantom has been used for both physical and computational representations of the human body, we use the term phantom only for physical phantoms that can be used within the framework of an experimental design. We then use the term model for a computational model that is defined on a computer for analytical or Monte Carlo calculations (5).

HISTORICAL DEVELOPMENTS

Because one cannot (easily) place a dosimeter within a live patient to measure the amount of radiation during a medical procedure, physical phantoms representing human anatomy were developed with tissue-equivalent materials that contain cavities for inserting small dosimeters. Users, however, soon realized that accurate measurements were time-consuming and costly, and the experimental effort required was often too great to be practical for large-scale and frequent applications. There were

cases in which the operators would be exposed to relatively large amounts of harmful radiation during the experiments. Using a different approach, researchers demonstrated that it is possible to represent the irradiation conditions and the human body in a mathematical way and to compute the dose distributions from knowledge of radiation-interaction processes using the well-established Monte Carlo methods (6).

One of the first applications of computer models of the human body for internal radiation dose assessment was performed during the Manhattan Project and published in the International Commission on Radiological Protection (ICRP) Publication 2 (7). The major focus at that time was the protection of radiation workers, and to a lesser extent the general public, from exposure to radioactive materials in connection with the war struggle. The proposed model of the human body and each of its parts was very crude, consisting simply of homogeneous spherical objects. The report was intended to cover the very large number of radionuclides for radiation safety purposes. This pioneering concept was used later by the ICRP in updated assessments for radiation workers, and found its way into other applications, such as dose assessments for nuclear medicine patients, thanks to the monumental efforts of the newly formed Medical Internal Radiation Dose (MIRD) Committee of the Society of Nuclear Medicine (SNM) in the United States (8).

Computational models have evolved from tissue-equivalent slabs or spheres homogeneous in composition and density to increasingly realistic anthropomorphic models that mimic the human body in both anatomy and composition. Currently, the computational models can be further classified as (*a*) mathematical-equation-based stylized models, in which organs are delineated by simple surface equations, or (*b*) image-based tomographic models, in which organs are defined from segmented medical images. A third class of hybrid models is now beginning to emerge that combines the first and second types of models. In the following, we describe these models in detail.

STYLIZED MATHEMATICAL MODELS

Early Stylized Models

As mentioned above, early mathematical specifications of human models developed ultimately for radiation-protection purposes mostly comprised homogeneous slabs, elliptical and right circular cylinders, and spheres (9, 10) and assumed a specific age, height, and weight. However, individuals' bodies and internal organs exhibit a variety of shapes and sizes. In the 1960s, researchers at Oak Ridge National Laboratory (ORNL) reported on the development of an adult model consisting of three specific regions: the head and neck; the trunk, including the arms; and the legs (11). The main limitations of this design are the crude approximations used to model the human body (mainly elliptical cylinders and truncated elliptical cones) and the inherent assumption of homogeneous tissue distribution. Likewise, organs such as the lungs and skeleton were not modeled, and the locations of specific organs in the model were not outlined. These developments were accompanied by the early designs of models representative of a pediatric population, including the newborn, 1-, 5-,

10-, and 15-year old (11). The main limitation of these designs (also known as the similitude pediatric models) is the crude assumption of the formalism used to construct the models, which presumes that children are simply small adults and consequently their organs are smaller adult organs (2). That is, these models were realized by applying a sequence of transformations to the major axes of the Cartesian coordinate system in which the adult model mentioned above was defined.

The first breakthrough in the history of computational models was the development of the Fisher-Snyder heterogeneous, hermaphrodite, anthropomorphic model of the human body in the late 1960s (12). This model, comprising three regions—skeleton, lungs, and the remainder (soft tissue)—was devised at ORNL for the SNM's MIRD Committee. Nine years later, Snyder et al. (13) published an improved version of the heterogeneous model. This stylized model consisted of spheres, ellipsoids, cones, tori, and subsections of such objects, combined to approximate the irregularly shaped regions of the body and its internal structures. It was analytically described in three principal sections: an elliptical cylinder representing the arms, torso, and hips; a truncated elliptical cone representing the legs and feet; and an elliptical cylinder representing the head and neck, as shown in **Figure 1**. The representation of internal organs with this mathematical model is very crude, as the simple equations can capture only the most general description of an organ's position and geometry. The original model developed was intended mainly to represent a healthy average adult male, which well characterized the working population of its time. The model had both male and female organs, but most structures represented the organs of the Reference Man (14), as defined by the ICRP from an extensive review of medical and other scientific literature, restricted primarily to European and North American populations. Note that the Reference Man was a 20- to 30-year-old Caucasian, 70 kg in weight and 170 cm in height (the height was later changed to 174 cm).

Current Stylized Models

Owing to the makeup of the nuclear medicine population and the diversifying worker population, the need for other models arose. In 1980, Cristy (15) of ORNL developed a series of models representing children of different ages, one of which (the 15-year-old) also served as a model for the adult female (16). For pediatric dosimetry, these models represented considerable progress over the similitude pediatric models referenced above. Later, Stabin et al. (17) released a set of models representing the adult female at different stages of gestation, to satisfy the need to calculate radiation doses to the fetus for nuclear medicine and other applications.

Since the first heterogeneous model referenced above was adopted by the MIRD Committee, a number of improvements to the model have been made over the following years and published in a series of MIRD pamphlets. Moreover, using the original descriptions, other investigators have developed modified versions such as those known as Adam and Eva (18). For many years, these stylized models have served practically as the de facto standard to the radiation-protection community (5, 19). In addition, other models were developed by the MIRD Committee and other independent investigators to represent certain organs or organ systems not included in these

Figure 1

Stylized adult male/female models showing (*a*) exterior view of the adult male, (*b*) skeleton and internal organs of the adult male/female, and (*c*) surface equations representing the stomach and gastrointestinal tract.

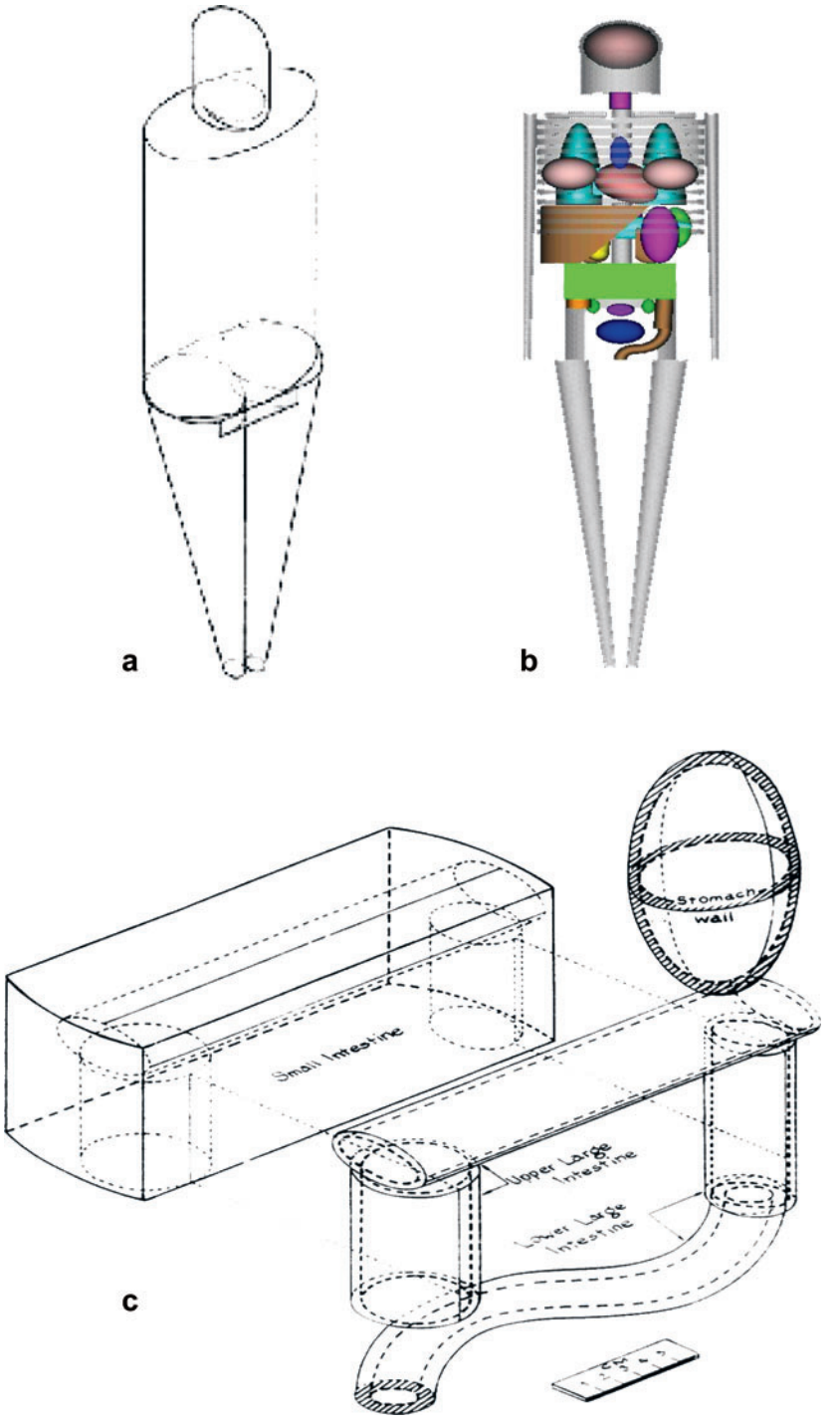

original models. Bouchet et al. (20) developed one adult and a series of five dosimetric head and brain models to allow for more precise dosimetry in pediatric neuroimaging procedures (21). Other models include subregions of the brain (22); the eye (23), nasal cavity, and major airway (24); the peritoneal cavity (25); the prostate gland (26); a new model of the nasal cavity and major airway (24); bone and marrow (27, 28); gastrointestinal (GI) tract (29) and a more recent refined rectum model (30); kidney (31); spheres of varying sizes simulating lesions (32, 33); and many others. To develop more patient-specific dosimetry that takes into account anatomical variability, new mathematical models for adults of different height have also been developed using anthropometric data (34, 35).

Many stylized models have been developed specifically for assessment of image-reconstruction techniques in CT and emission tomography and may not be suitable for other applications in radiological sciences (e.g., radiation dosimetry). Examples of these include the popular Shepp-Logan brain model (36), which has been used extensively during the early development of image-reconstruction methodologies, and the FORBILD (Bavarian Center of Excellence for Medical Imaging and Image Processing) database developed by the Institute of Medical Physics of Erlangen University, Germany (37). The latter family of objects comprises various organ models representing the head, abdomen, lung, thorax, hip, and jaw.

Dynamic (4-D) Stylized Models

Mathematical anthropomorphic models are continuously being improved. Recent advances in three- and four-dimensional models (i.e., 3-D spatial computer models incorporating accurate modeling of time-dependent geometries requiring high temporal resolution) are a result of necessary compromise of complexity, anatomical accuracy, ease of use, and flexibility. Current developments are aimed at computer models that are flexible while providing the accurate modeling of patient populations. The use of dynamic anthropomorphic models in Monte Carlo simulations is becoming possible, owing to the increasing availability of computing power. Paganetti et al. (38) reported on the simulation of time-dependent geometries within a single 4-D Monte Carlo simulation using the geometry and tracking (GEANT4) Monte Carlo package. This is made possible through the development of appropriate primitives that allow the accurate modeling of anatomical variations and patient motion, such as superquadrics (39) and nonuniform rational B-spline surfaces (NURBS) (40, 41). Superquadrics are a family of 3-D objects such as superellipsoids and tori that can be used to efficiently model a variety of anatomical structures. Their usefulness in modeling heart and thorax models has been demonstrated both in CT (42) and emission tomography imaging techniques (39). The former reference particularly emphasized that superquadric modeling provides a more realistic visualization than quadratic modeling and a faster computation than spline methods. Considerable research efforts are also being spent to develop integrated frameworks, allowing tumor growth models to be linked into anthropomorphic models in which the tumors are approximated either by analytically defined 5-D (x, y, z, $t_{geometry}$, $t_{activity}$) compartments or by compound cellular lattice inserts (43).

Segars and colleagues' (41) 4-D NURBS-based Cardiac-Torso (NCAT) model brought several improvements to the earlier Mathematical Cardiac-Torso (MCAT) anthropomorphic model (44) used extensively in emission-CT imaging research. The latter uses mathematical formulae; the size, shape, and configurations of the major thoracic structures; and organs such as the heart, liver, breasts, and rib cage to achieve realistic modeling. Incorporation of accurate models of cardiac and respiratory physiology into the current 4-D NCAT model was a significant step forward to account for inherent cardiac and respiratory motion not considered in the previous models. The conceptual design of this model also served as a basis for development of the 4-D digital mouse model termed MOBY (mouse whole body) (45), which is based on high-resolution gated magnetic resonance microscopy acquired data and NURBS formalism (40), mentioned above for modeling the organ shapes. Three-dimensional surface renderings illustrating anterior and lateral views of the digital mouse model are shown in **Figure 2**. The NURBS primitives can elegantly model the complex organ shapes and structures, providing the foundation for a realistic model of the 3-D mouse anatomy.

TOMOGRAPHIC VOXEL-BASED MODELS

Stylized models described previously are mathematically defined using second-order quadratic surface equations. For example, the stomach wall (the American football shape in **Figure 1*c***) is defined as the volume between two concentric ellipsoids (16):

$$\left(\frac{x-x_0}{a}\right)^2+\left(\frac{y-y_0}{b}\right)^2+\left(\frac{z-z_0}{c}\right)^2 \leq 1$$

$$\text{and} \quad \left(\frac{x-x_0}{a-d}\right)^2+\left(\frac{y-y_0}{b-d}\right)^2+\left(\frac{z-z_0}{c-d}\right)^2 \geq 1.$$

Over time, the stylized models had been revised by different researchers, for example, by subdividing the head/brain regions (46). However, despite efforts to revamp the stylized models, the representation of a patient's body remained anatomically unrealistic owing to the geometric limitation of these quadratic equations. The development of anatomically realistic models was desirable but impossible until tomographic medical imaging modalities became available. CT and MRI allow us to visualize the internal structures of the body in three dimensions and to store the images in versatile digital formats. The medical communities immediately took advantage of using these 3-D tomographic images to improve treatment planning and dose assessment and to validate methodologies, allowing improved image quality and quantitative accuracy of medical imaging techniques. Compared with the medical applications, however, the task of developing well-defined standard human models faced some unique and intractable technical challenges: (*a*) Whole-body models are needed, but medical images are often taken for a portion of the body (CT procedures expose the patients to intense X rays, and MRI is time-consuming). (*b*) A large amount of internal organs/tissues have to be identified and segmented for organ dose calculations for systematic dose calculations, whereas, in radiotherapy, for example, only the tumor volume and adjacent regions need to be outlined. (*c*) The image data size of

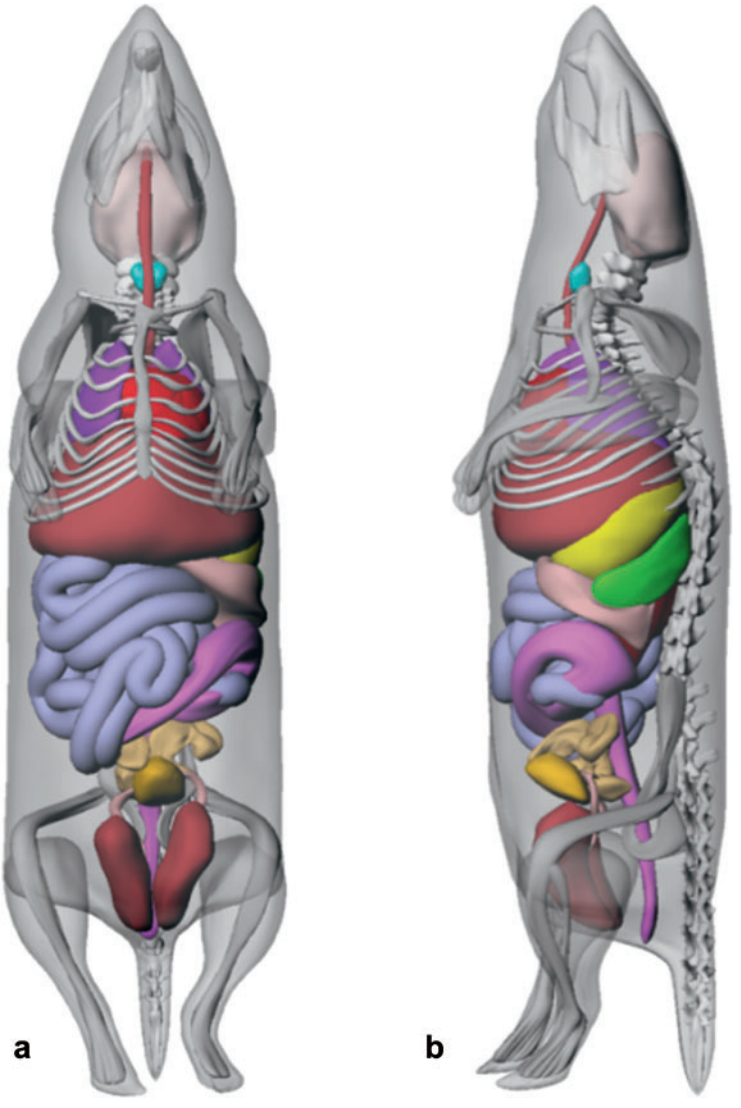

Figure 2

3-D surface renderings showing anterior (*a*) and lateral (*b*) views of the 4-D digital mouse phantom (MOBY). Reprinted with permission from Reference 45.

a whole-body model can be potentially too big for a computer's memory to handle. (*d*) A standardized patient model involves dose calculations for photons, electrons, neutrons, and protons, but the majority of the clinical procedures involve fewer types of radiation.

CT imaging offers excellent contrast for the skeleton as well as many other major organs without the use of contrast agents in a live subject. CT imaging is also much faster than MRI, and the newly available multidetector CT systems (up to 64-slice CT capability) can produce submillimeter slices in a few seconds. Given the fact that the radiation exposure from a whole-body CT procedure normally

results in acceptably low doses, the use of MRI offers no distinct advantages except for certain situations involving soft tissues. In addition to the use of medical imaging of live subjects, anatomical information has been obtained from cadavers. The body of a cadaver can be imaged by CT or MRI in the same way as a live subject, but unique anatomical details are also available from cross-sectional color photography. Cadaver imaging allows the entire body to be covered at desired slice thickness. The Visible Human Project (VHP), sponsored by the U.S. National Library of Medicine, for example, produced anatomically similar CT, MRI, and cross-sectional color photographs (47). For many years, the VHP color images had the smallest voxel size (the male at 0.33 mm × 0.33 mm × 1 mm, and the female at 0.33 mm × 0.33 mm × 0.33 mm, which were much better than those available in the 1990s from CT or MRI) until the Chinese VHP published a set of segmented color photographs at 0.1 mm × 0.1 mm × 0.2 mm voxel size for a male cadaver recently (48). However, cadaver imaging is related to some unfavorable conditions, including deformation of organs due to a clinical cause such as a trauma or the process to prepare the body for imaging.

In terms of geometrical descriptions, the tomographic models are fundamentally different from the stylized models. Generally, medical images consist of pixels (picture elements), each representing a tissue volume in a 2-D plane. The 3-D volume of the tissue is termed a voxel (volume element), and it is determined by multiplying the pixel size by the thickness of an image slice. Unlike stylized whole-body models, a tomographic model (also termed voxel model) contains a huge number of tiny cubes grouped to represent each anatomical structure.

The creation of a tomographic model involves four general steps: (*a*) Acquire a set of medical images, (*b*) classify and segment the organs or tissues of interest for the application at hand (e.g., lungs, liver, skin, etc.) from the original images by assigning voxels with unique identification numbers, (*c*) specify tissue type (e.g., soft tissue, hard bone, air, etc.) and composition to organs or tissues, and (*d*) implement the geometric data into a Monte Carlo code to calculate radiation transport and score quantities of interest (e.g., dose in each of the organs of interest). The segmentation of original images into organs and tissues often requires a very time-consuming and laborious manual process (there are some cases where automatic methods are possible), often taking months or years to complete. In general, the creation of a tomographic model means the completion of all these above four steps. Currently, there is no consensus on what constitutes a true segmentation because the process often involves some level of assumption about the anatomy during the image analysis. For example, the GI tract has poor CT image contrast, and the segmentation is often very difficult or even impossible without the use of a contract agent. For very small organs such as skin, which is less than 1 mm thick, a typical CT or MR image dataset at more than 2 mm × 2 mm pixel resolution is not fine enough to delineate the thin skin layers in various parts of the body. As a result, most existing tomographic models assume that the skin is made of the top layer of the voxels, which create a skin that is too thick. The segmentation of the red bone marrow from images is so hard that most models (except for the VIP-Man model described below) define it using an empirical formula to calculate it instead of direct 3-D modeling.

There is also an interesting issue related to the intellectual property of this research. It is not clear who should own the right of naming a model because the four steps discussed above can be carried out by different individuals. One scenario is when the original images were acquired and segmented by one individual and then when a different individual performed additional image processing and modification before implementing the data into a specific Monte Carlo code. Such changes produce a practically unique final radiological imaging or radiation dosimetry model, and proper naming indicating any major changes is necessary for future comparisons of imaging or dosimetry data.

Existing Tomographic Models

Since 1988, a number of research groups have developed and reported tomographic models based mostly on CT images of live subjects. Adult male models were first developed. Later, adult female, pediatric, and pregnant-women models were also developed. **Table 1** summarizes more than 30 whole-body tomographic models that have been reported in the literature. These models contain organs that are segmented and classified and thus ready for implementation into a Monte Carlo code. **Table 1** is an updated version of that from a recent review paper (49).

A clinically realistic brain model simulating source distributions in the human brain—typical in cerebral blood flow and metabolism studies employed in PET, providing apparent relative concentrations of 4, 1, and 0 for gray matter, white matter, and ventricles, respectively, in functional brain imaging—was developed (50) on the basis of the physical Hoffman 3-D brain phantom (51). Zubal et al. (52) from Yale University published a head-torso model from CT images named VoxelMan. Their original goal was to create a tomographic computational model for optimizing nuclear medicine imaging. The original CT images consisted of two sections with different pixel resolutions: one of 78 slices from the neck to midthigh with 10-mm-thick slices, and one of 51 slices from the head to the neck region with 5-mm slices. After reprocessing the images, the final tomographic model has a uniform voxel size of 4 mm × 4 mm × 4 mm. The same group has also developed a high-resolution brain phantom based on an MRI scan of a human volunteer, which can be used for detailed investigations in the head. The torso phantom was further improved by copying the arms and legs from the VHP and attaching them to the original torso phantom (53). However, the arms of the VHP cadaver were positioned over the abdominal part, which limited the usefulness of the phantom for simulations of whole-body scanning. This problem was tackled by mathematically straightening the arms out along the phantom's sides (54). On the basis of Zubal's original image data, Kramer et al. (55) from Brazil recently developed a male adult voxel model named MAX (Male Adult voXel) for Monte Carlo calculations and a female adult model named FAX (56).

Dimbylow (57, 58) from the National Radiological Protection Board (NRPB), United Kingdom, developed an adult male model known as NORMAN using magnetic resonance images of 2 mm × 2 mm resolution and 10-mm-thick slices. NORMAN was first used by Dimbylow with finite-element simulation code to determine the specific energy absorption rate from exposure to nonionizing

Table 1 Existing tomographic and hybrid human models with their main characteristics

Developer	Name	Images	Race	Age and sex	Subject	Comment	Reference
Flinders University, Australia	ADELAIDE	CT	Caucasian	14-year-old female	Patient	Torso	(64)
Federal University of Pernambuco, Brazil	MAX	CT	Caucasian	Adult male	Patient	VoxelMan with arms and legs added	(55)
Federal University of Pernambuco, Brazil	FAX	CT	Caucasian	Adult female	Patient		(56)
Federal University of Pernambuco, Brazil	MAX06, FAX06	CT	Caucasian	Adult male and female	Patient	MAX06 has skeleton based on the FAX; adjusted to ICRP 2005	(79)
GSF, Germany	BABY	CT	Caucasian	8-week-old female	Cadaver		(63)
GSF, Germany	CHILD	CT	Caucasian	7-year-old female	Leukemia patient	Small for age (5- to 7-year-old)	(63)
GSF, Germany	DONNA	CT	Caucasian	40-year-old female	Patient		(61, 62)
GSF, Germany	FRANK	CT	Caucasian	48-year-old male	Patient	Head and torso	(61, 77)
GSF, Germany	GOLEM/ICRP	CT	Caucasian	38-year-old male	Leukemia patient	Adjusted to ICRP 2005	(109, 110)
GSF, Germany	HELGA	CT	Caucasian	26-year-old female	Patient	Legs absent below midthigh	(62, 77)
GSF, Germany	IRENE	CT	Caucasian	32-year-old female	Patient		(62, 77)
GSF, Germany	LAURA/ICRP	CT	Caucasian				(77)
GSF, Germany	VISIBLE MAN	CT	Caucasian	39-year-old male	Cadaver (VHP)	No arms	
NIICT, Japan	Nagaoka Man	MRI	Japanese	22-year-old male	Volunteer		(67)
NIICT, Japan	Nagaoka Woman	MRI	Japanese	22-year-old female	Volunteer		
JAERI, Japan	Otoko	CT	Japanese	Adult male	Healthy volunteer		(68)
JAERI, Japan	Onago	CT	Japanese	Adult female	Healthy volunteer		
JAERI, Japan	JM	CT	Japanese	55-year-old male	Healthy volunteer		(69)
JAERI, Japan	JF	CT	Japanese	Adult female	Healthy volunteer		(70)
Johns Hopkins University, USA	NCAT	CT	Caucasian	39-year-old male	Cadaver (VHP)	No arms; motion simulating	(41)
Hanyang University, Korea	KORMAN	MRI	Korean	28-year-old male			(71)

Lund University, Sweden	VOXTISS8	CT	Caucasian	Adult male	Patient	MANTISSUE3-6 with arms mathematically straightened along the model's side	(54)
NRPB, UK	NORMAN	MRI	Caucasian	Adult male		Only 10 ribs	(57, 59)
NRPB, UK	NAOMI	MRI	Caucasian	Adult female	Healthy volunteer		(60)
ENEA-ION Istituto di Radioprotezione, Italy	NORMAN-05	MRI	Caucasian	Adult male		Adjusted to ICRP 2005	(80)
RPI, USA	Pregnant woman	CT		30 weeks pregnant		Part torso	(75)
RPI, USA	VIP-Man	Color photos	Caucasian	39-year-old male	Cadaver (VHP)	One testicle only	(72)
RPI, USA	VIP-Man 4D	Color photos	Caucasian	39-year-old male	Cadaver (VHP)	Only chest; motion simulating	(103)
UF, USA	UF 2 month	CT	Caucasian	6-month-old male	Cadaver		(65)
UF, USA	UF newborn	CT	Caucasian	6-day-old female	Cadaver		
UF, USA	UF 9 month	CT		9-month-old male	Patient	Head and torso	
UF, USA	UF 4 year	CT		4-year-old female	Patient		(66)
UF, USA	UF 8 year	CT		8-year-old female	Patient		
UF, USA	UF 11 year	CT		11-year-old male	Patient		
UF, USA	UF 14 year	CT		14-year-old male	Patient		
University of Victoria, Canada	MANTISSUE3-6	CT	Caucasian	Adult male	Patient	VoxelMan with arms and legs added from VHP	(53)
Yale University, USA	VoxelMan	CT	Caucasian	Adult male	Patient	Head and torso	(52)

electromagnetic fields. His colleague from NRPB, Jones (59), adopted NORMAN to estimate organ doses from external and internal photon sources. Dimbylow later developed an adult female model, NAOMI, from 2-mm-pixel MRI scans (60). The model was rescaled to a height of 1.63 m and a mass of 60 kg, the dimensions of the ICRP reference adult female. To date, the NAOMI model has been used only in nonionizing radiation calculations.

Zankl et al. (61, 62) from the National Research Center for Environment and Health (GSF), Germany, developed a family of nine tomographic models, all from CT images: BABY, CHILD, DONNA, FRANK, GOLEM, HELGA, IRENE, LAURA, and VISIBLE MAN. However, the earlier models, such as the adult male GOLEM, had relatively poor image resolution (e.g., 2 mm × 2 mm) and large slice thickness (e.g., 8 mm). The BABY and CHILD models were one of the first nonadult models (63). The resolutions for BABY and CHILD are 0.85 mm × 0.85 mm × 4 mm and 1.54 mm × 1.54 mm × 8 mm, respectively. Caon et al. (64) from Flinders University, Australia, reported a partial-body model named ADELAIDE, which represents a 14-year-old girl. Recently, Bolch and colleagues (65, 66) from the University of Florida created a series of pediatric models ranging from the first year of life to 14 years old.

Two Japanese groups have recently been active in developing tomographic models. Nagaoka et al. (67) from the National Institute of Information and Communications Technology (NIICT) reported an adult male model, named Nagaoka Man, and an adult female model, named Nagaoka Woman, developed from magnetic resonance images for radio-frequency electromagnetic-field dosimetry. Saito et al. (68–70) from the Japan Atomic Energy Research Institute (JAERI) developed an adult male model, named Otoko, and a female model, named Onago, as well as two more recent models aimed mainly for radiation dosimetry applications. Lee & Lee (71) from Hanyang University recently reported a Korean adult male model by using magnetic resonance images. Other countries, including India and China (48), are reportedly also developing their own tomographic models.

Xu and colleagues (72) from Rensselaer Polytechnic Institute focused initially on an adult male model termed VIP-Man, which was based on cross-sectional color photographic images for a 39-year-old male cadaver from the VHP. **Figure 3*a*** contrasts the striking anatomical differences between the cross-sectional views of the VIP-Man model with the stylized model. **Figure 3*b*** and **3*c*** are 3-D surface renderings of the VIP-Man model, showing anatomical realism of the trunk and head, respectively. The transversal anatomical images were obtained during the VHP by photographing the top surface of the body block after removal (by shaving) of each successive millimeter (0.3 mm for the female cadaver) by a cryomacrotome (47). Each anatomical photograph represents a 1-mm-thick slice of the male cadaver.

The VIP-Man model consists of more than 3.7 billion voxels, and the original images were segmented to yield more than 1400 organs and tissues, although only approximately 80 were adopted for radiation dosimetry applications (47, 72). Automatic and manual image processing and segmentation were performed by Xu and his students at Rensselaer to obtain gray matter, white matter, teeth, skull, cerebrospinal fluid (CSF), stomach mucosa, male breast, eye lenses, and red bone marrow (72). Traditional image-processing techniques were employed to identify tissues on the

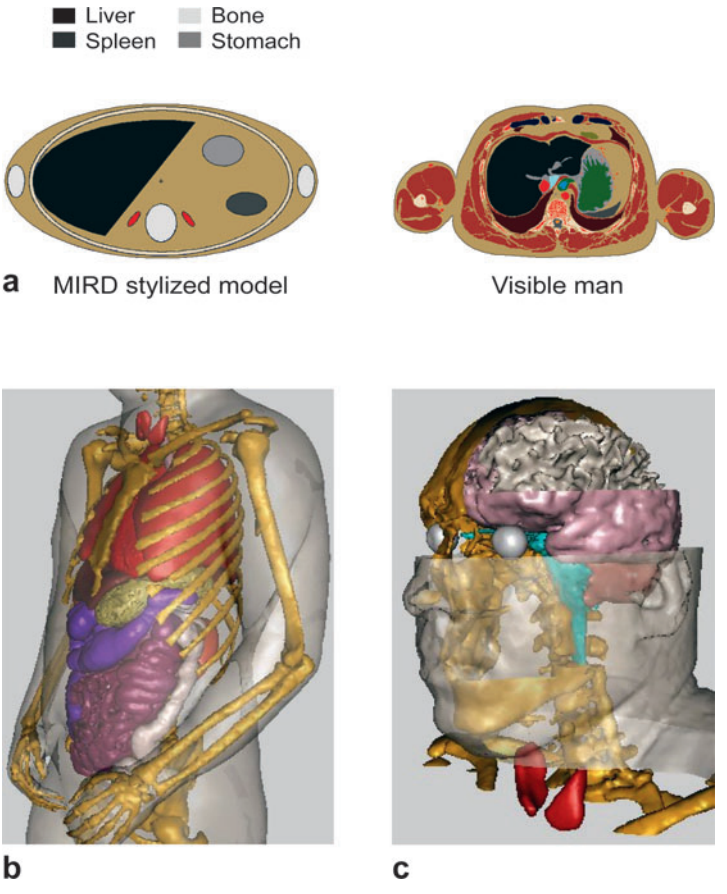

Figure 3

(*a*) The anatomical representation of the VIP-Man model is obviously different from the stylized model. (*b*) VIP-Man in 3-D view, showing details of internal organs and the skeleton. (*c*) VIP-Man in 3-D view, showing details of the head and brain.

basis of color separation (for example, redness for red bone marrow). GI track mucosa was realistically represented, except for the stomach, where one voxel layer on the inner surface of the wall was used. The final list covers critical organs or tissues of interest to radiological sciences. Other organs or tissues are included because of their potential roles in biomedical engineering applications. Once an organ or tissue has been segmented, the associated voxels could be arbitrarily labeled or colored for visualization.

These data covered the entire body, with each voxel having a small size of 0.33 mm × 0.33 mm × 1 mm for the male. The small voxel size in this model allowed many small organs and tissues to be represented, or represented more accurately, compared with the other models. The finalized VIP-Man model shows a heavy body weight of 103 kg (due to a relatively large portion of fatty tissues), and was considered to be an ideal model for studying how much a specific individual can deviate anatomically from the Reference Man (14). Note that most organs in VIP-Man have similar masses as those of the Reference Man. If necessary, the excessive fat tissue can be removed, and the size/shape of many organs in the VIP-Man model

can be individually adjusted to match closely with the Reference Man. Several critical breakthroughs on handling the huge image data were made, and the VIP-Man model has been successfully implemented in various Monte Carlo codes, including MCNP, MCNPX, EGS, and GEANT4, for internal and external organ dose calculations involving photons, electrons, neutrons, and protons (see **http://RRMDG.rpi.edu**). In addition, the VIP-Man model has been used to assess X-ray image quality (73) and in surgical simulation (74).

Shi & Xu (75) also developed an eight-months-pregnant woman model from CT images, which has been used to derive specific absorbed fractions for nuclear medicine applications (76). In addition to the color photographs, CT and magnetic resonance images were also taken for the same VHP subject. The VHP CT images were used to develop the VISIBLE MAN model at GSF (77) and the 4-D NCAT model (41).

The ICRP is currently finalizing new recommendations that call for a paradigm change from the stylized models to tomographic models (78). In addition, a number of new organs and tissues are now included in the list for calculating the effective dose, a fundamental quantity in radiation-protection dosimetry. In response to these proposed changes, a number of researchers have further revised previously published tomographic models. Kramer et al. (79) introduced the MAX06 and FAX06, which are based on the MAX and FAX models, respectively. In their work, adjustment of organ and tissue masses was attempted to agree as closely as possible with the new ICRP-recommended anatomical values. Particular attention was paid to the total skeletal masses and volumes, and the new models contain skeletons that have been segmented into spongiosa, cortical bone, medullar yellow bone marrow in the shafts of the long bones, and cartilage and miscellaneous tissues. In addition, a major change was made to the MAX06, whose skeleton is now based on the skeleton of the FAX. Ferrari & Gualdrini (80) from the Istituto di Radioprotezione, Bologna, Italy, recently made similar adjustments to one of the first adult male tomographic models, NORMAN (57). The revised model, named NORMAN-5, was used to calculate photon fluence-to-dose-conversion coefficients. In these two recent papers, a direct comparison with the ICRP standard voxel model to show the potential uncertainties in dosimetry could have been useful to the radiation-protection community. Unfortunately, such a comparison is not addressed in these papers, partly because the ICRP standard models are still being adjusted at GSF.

Red Bone Marrow Dosimetry Model

Radiation dosimetry for the bone marrow has been an important research topic in radioimmunotherapy, which treats cancer patients by injecting monoclonal antibodies labeled with charged-particle-emitting radionuclides. A tomographic model of the red bone marrow 3-D distribution, coupled with Monte Carlo methods, can provide a ground truth to allow for comparison of various empirical methods of red bone marrow dosimetry, such as those discussed by Lee et al. (81).

The marrow cavities in the trabecular bone have a linear dimension in the range of 50 to 2000 microns (82). The red (active) bone marrow occupies merely a portion of these marrow cavities, determined by the cellularity factor for the bone under

consideration (83). Given the voxel size of 0.33 mm × 0.33 mm × 1 mm in the VHP color images, it appears that a direct segmentation of these images will not yield 100%-accurate marrow cavities because the voxels are not smaller than the dimensions of all of the objects. However, if the basis of the segmentation is the red color contents in each pixel (i.e., information related directly to the red bone marrow without inactive yellow marrow), then a global calibration factor can be employed to determine whether a pixel should be identified as a part of the red bone marrow. The global calibration factor reflects the clinically determined total red bone marrow fraction in a bone (84). Note that this approach is not meant to segment spongiosa (i.e., trabecular bone + marrow). Instead, it is meant to separate the red bone marrow from the original VHP images using both the color-analysis scheme and information for the total red bone marrow fraction in a bone. This unique approach is different from the method of using Hounsfield numbers in a CT image that does not differentiate red from yellow marrows.

Therefore, using the VHP color images and the approach described above, the accuracy of the modeled spatial red bone marrow distribution inside an entire skeleton system can be ensured. In other words, such a red bone marrow model provides an estimated red bone marrow distribution of the active marrow at a macroscopic level (above 330 microns). Obviously, microscopic images with pixels less than 50 microns, such as those obtained from micro-CT, would be ideal for modeling the marrow cavities (85). However, currently, micro-CT images are available for only a few selected bone locations, not the entire skeleton. The red bone marrow model in VIP-Man is the only reported attempt to directly model the 3-D active marrow distribution in the entire skeleton—information that is necessary for many radiation-transport and dosimetry studies involving irradiation of the whole body. The availability of identical cross-sectional color images and CT images from the VHP allow unique dosimetric investigations. For example, the red bone marrow distribution in the color images can be used to benchmark a generic method of segmenting this tissue from the CT, which is widely available in the clinical setting (84).

Recent Efforts to Develop the International Commission on Radiological Protection Reference Tomographic Models

Since 1998, the ICRP's Task Group on Dose Calculations (DOCAL) and the SNM's MIRD Committee have been evaluating new dosimetry data from these tomographic models. In particular, the DOCAL, which is administered by the ICRP Committee 2, has been developing international guidelines on the use of voxel-based models. In an ICRP annual report in 2002 (p. 10, 86), a paradigm shift in the way the human body is modeled for radiation-protection dosimetry was predicted: "An important issue for Committee 2 is the substitution of an anatomically realistic voxel phantom, obtained digitally in magnetic resonance tomography and/or computed tomography, for the MIRD phantom which is a mathematical representation of a human body."

The ICRP has decided to develop these new reference models using the following strategy: (*a*) Select a CT image dataset of persons close to the Reference Man (height and weight), (*b*) segment the dataset, (*c*) adjust body height to reference value by

scaling voxels, (*d*) adjust skeletal mass to reference value, and (*e*) adjust individual organs to reference values by addition/subtraction of voxels. The ICRP has decided to adjust the GOLEM and LAURA models developed previously at GSF. Final adjustments are being made with regard to data published in ICRP Publication 89 (87) and the draft ICRP 2005 Recommendations (78). The ICRP is expected to release the guidelines and finalized ICRP standard models in the beginning of 2007. In one attempt to bring together researchers working on tomographic models, a special conference session, "Tomographic Models for Radiation Protection Dosimetry," was organized during the Proceedings of the Monte Carlo Method: Versatility Unbounded in a Dynamic Computing World in Chattanooga, Tennessee. Ten researchers from different countries were invited to report on the latest research and the ICRP's recommendations on tomographic models. During the conference, attendees formed the Consortium on Computational Human Phantoms (CCHP; **http://www.virtualphantoms.org**) to facilitate research collaboration and dissemination. It is expected that, in the future, the CCHP will become a center of resources for human anatomy modeling.

RELEVANCE OF REALISTIC MODELS IN MONTE CARLO SIMULATIONS OF RADIOLOGICAL IMAGING SYSTEMS

Patient anatomical modeling is fundamental for performing photon and electron dosimetry accurately and efficiently by means of a Monte Carlo method. The modeling process consists of a description of the geometry and material characteristics for an object. The material characteristics of interest include composition, density, and energy-dependent cross sections. Simulation of medical imaging systems using deterministic methods and simplifying approximations have been developed mainly to improve speed of operation. However, the use of the Monte Carlo method for radiation transport simulation, although time-consuming, has emerged as the most accurate means of simulating patient exposure conditions. These simulations represent a typical scanning procedure by using an imaging modality with the aim of optimizing instrumentation design or predicting absorbed dose distributions and other quantities of interest in diagnostic procedures and radiation treatments of cancer patients (1, 6). This trend has continued for the assessment of image quality and the quantitative accuracy of both anatomical and radionuclide imaging. There has been an enormous increase and interest in the use of Monte Carlo techniques in all aspects of radiological sciences, covering almost all topics including detector modeling and imaging systems design, development and evaluation of image-correction and reconstruction techniques, and internal dosimetry and pharmacokinetic modeling (1), with an increasingly enthusiastic interest in exotic and exciting new applications such as online PET monitoring of radiation therapy beams (88).

Monte Carlo simulations are very useful for the development, validation, and comparative evaluation of image-correction and reconstruction techniques because it is possible to obtain a reference image to which corrected/reconstructed images should be compared. The interest in fully 3-D Monte Carlo–based statistical reconstruction

approaches spurred the development of computationally efficient algorithms capable of obtaining highly accurate quantitative data in clinically acceptable computation times (89). However, the capability to theoretically model the propagation of photon noise through emission-CT reconstruction algorithms is fundamental to evaluating both the quality and quantitative accuracy of reconstructed images as a function of the parameters of the algorithm. Monte Carlo methods can be used to check the validity of the predictions of the theoretical formulations through computing the sample statistical properties of the algorithms under evaluation (90).

Monte Carlo calculations are also powerful tools for quantifying and correcting for partial-volume effect, photon attenuation, and scattering in nuclear medicine imaging because the user has the ability to separate the detected photons into their components: primary events, scatter events, contribution of down-scatter events, and so on. Monte Carlo modeling thus allows a detailed investigation of the spatial and energy distribution of Compton scatter, which would be difficult to perform using present experimental techniques, even with very good energy-resolution semiconductor detectors. A recent review by Zaidi & Koral (91) extensively describes modeling the scatter-response function and development and assessment of scatter-correction methods in both SPECT and PET using Monte Carlo simulations.

Several studies addressed the issue of the impact of scatter in radionuclide transmission and X-ray CT scanning, as well as the influence of down-scatter from emission (e.g., ^{99m}Tc) to transmission (e.g., ^{153}Gd) data on the accuracy of the derived attenuation map in emission tomography. The comparative assessment of different attenuation-correction strategies in lung (92) and brain (93) SPECT studies was also conducted using Monte Carlo simulations of a digital thorax and brain computational models, respectively. The same head/brain model used in the latter was employed for deriving a patient-specific attenuation map by registering the brain component of the digital-head atlas (52) with a source distribution of 4:1:0 for gray matter, white matter, and ventricles, respectively, to a preliminary PET reconstruction and then applying the resulting spatial transformation to the anatomical-head atlas (94). The latter was used to construct a patient-specific attenuation map by assigning known attenuation coefficients to different head tissues.

Monte Carlo simulations are also powerful tools to investigate the limits of algorithms developed for correction of partial-volume effect by allowing the replication of realistic conditions in emission tomography for a wide range of practical situations, and to study the effect of object shape and size on recovery performance (95). In addition, the assessment of the impact of inherent assumptions such as accurate characterization of system response function, perfect registration between MRI/CT and PET/SPECT, and anatomical-image segmentation, as well as other hypotheses regarding tracer distribution on quantification bias, is more straightforward compared with experimental approaches (96).

Computing power is now quite vast; computers sitting on our desktops today hold more power than those available only in privileged major research institutions some 20 years ago. Dedicated workstations and distributed computing networks continue to increase in size and power by orders of magnitude every few years. Many

Monte Carlo computer programs have been in use in the field of radiological imaging and radiation dosimetry, with some of them available as open source codes in the public domain. Basically, there are two categories of software packages: general-purpose Monte Carlo codes developed for high-energy physics research, or general medical physics applications and dedicated software packages developed mainly and optimized for a specific application in radiological sciences. These are highly sophisticated tools requiring advanced computer skills and familiarity with radiation transport theories. Each category has its own advantages and drawbacks, and the choice of a particular code is dictated by the availability of the code and documentation, the physics and geometry related to the application, and the user's experience. Two examples of codes developed at one of the authors' (H.Z.) laboratory are briefly described below as snapshots of the dynamically changing field of Monte Carlo simulation of medical imaging systems using the anatomical models reviewed in this paper.

An example of dedicated Monte Carlo codes is the *Eidolon* simulator, which was developed using modern software-engineering techniques mainly for fully 3-D multiring PET imaging (97). The code was written in Objective-C, an object-oriented programming language based on American National Standards Institute (ANSI) C (98). A modular software architecture featuring dynamically loadable program elements or bundles was adopted in software design. The basic building block is a model-element object class, which allows the user to select scanner parameters such as the number of detector rings, detector material and sizes, energy-discrimination thresholds, and detector energy resolution. It also allows the user to choose either a complex anthropomorphic model or a set of simple 3-D shapes, such as parallelepiped, ellipsoid, or cylindrical, for both the annihilation sources and scattering media, as well as their respective activity concentrations and chemical compositions. An implementation of the software on a high-performance parallel platform was also reported (99). The current version runs on most of the current platforms and operating systems supporting the GNU C compiler, which should allow subdividing time-consuming simulations on geographically distributed platforms, taking advantage of the latest developments in Grid technology (see **http://pinlab.hcuge.ch/**).

Another example is the X-ray CT Monte Carlo simulator based on the MCNP4C radiation transport computer code developed for simulation of fan- and cone-beam CT scanners (100). A user-friendly interface running under Matlab (The MathWorks Inc.) creates the scanner geometry at different views as MCNP4C's input file. The full simulation of X-ray tube, collimator, bow-tie filter, object model, and detector geometry and material with single-slice, multislice, and flat-panel detector configurations was considered (101). **Figure 4** illustrates the principles and main components of the MCNP4C-based Monte Carlo simulator as applied to modeling an X-ray CT imaging system. The simulator was validated using experimental measurements from different phantoms containing steel, Teflon, water, polyethylene, and air cylinders, with different sizes on a clinical fan-beam scanner and a small-animal cone-beam CT scanner, and is now being used extensively for development and assessment of sources of error and artifact when using CT-based attenuation correction in dual-modality PET/CT imaging systems (102).

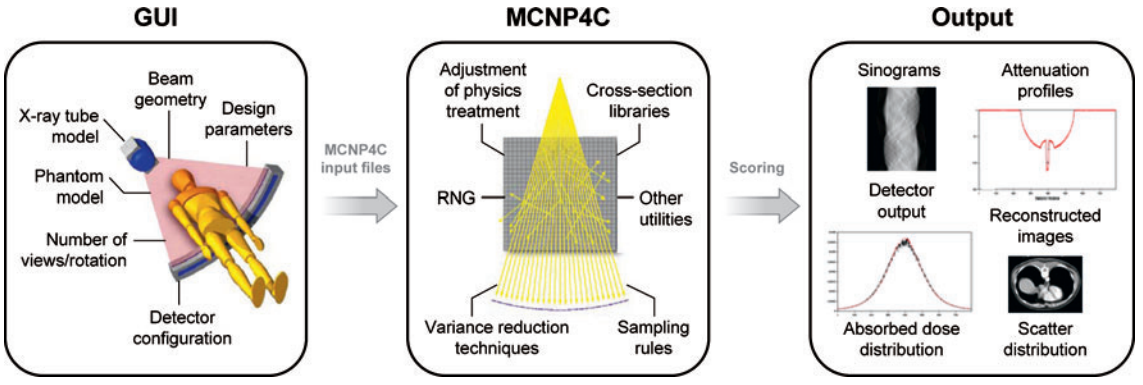

Figure 4

Principles and main components of the MCNP4C-based Monte Carlo program dedicated to simulation of X-ray CT imaging systems.

FUTURE DIRECTIONS

Clearly a new generation of human modeling tools needs to be developed for use with simulation of radiological imaging systems and dosimetry calculations. It is unfortunate to use, in the twenty-first century, standardized, stylized models to perform dose calculations for individual patients if meaningful information to be used in the assessment of potential radiation hazard or in planning patient therapy is sought. The evolution of the methodology followed for external-beam radiotherapy treatment planning is now finding its way to targeted therapy. The technology, based on the fusion of anatomical (CT or MRI) and functional (SPECT or PET) data, now exists to develop patient-specific 3-D dose distributions, with individualized Monte Carlo calculations done in a reasonable amount of time using high-powered computing workstations or distributed computing networks. The combination of realistic computational models of the human anatomy with accurate models of the imaging process allows the simulation of radiological imaging data ever closer to actual patient data. Modeling techniques will find an increasingly important role in the future of radiological sciences in light of the further development of realistic computational models, the accurate modeling of radiation-interaction processes, and computer hardware. However, caution must be taken to avoid errors in the modeling process, and verification via comparison with experimental and patient data is essential.

Voxel-based geometry lacks the flexibility for organ adjustment and is hardly the ideal form for human-body modeling. An ongoing research topic aims to develop models that address problems associated with cardiac and respiratory motions during medical imaging and radiation therapy (38). Organ motions involve tissue deformation—a process difficult to handle using a voxel-based data format. The new approach combines voxel data with a NURBS approach to design a third type of human model, termed hybrid models, whose organ shapes are more realistic than stylized models but maintain the flexibility for anatomical variations and organ deformation. In this type of voxel and equation hybrid models, one can adjust the NURBS surface

control points of an organ to the desired shape and volume using patient-specific images and deformable-image-registration techniques. Examples of such hybrid models include the 4-D NURBS-based NCAT model for cardiac imaging simulations, which uses the VHP CT images (41), and the 4-D VIP-Man model for respiratory motion management during radiation treatment planning, which uses the VHP anatomical color images (103).

Despite more than 30 tomographic models having been developed, improvements brought by these models in operational radiation protection may be considered insignificant for the most common radiation exposure scenarios. A key reason for the lack of real improvement is the continued employment of the Reference Man concept in radiation protection, where two standard models are used universally as an average of the populations (14, 104). The biggest advantage of tomographic models is the potential for realistic and person-specific radiation dosimetry. The development of new whole-body tomographic models will likely continue in the future; however, the community should focus on models that fill certain ethnic and/or age groups, contain new organs, or provide additional features such as cardiac and respiratory motion simulations for advanced modeling of the lungs and the heart. Also in need of further attention is the comparison among different models, especially with the new ICRP standard models to be released in the near future. One of the most promising research topics is advanced and user-friendly computer tools to facilitate the adjustment of the body and organs to any desired patient-specific shape and size. New capabilities in simulating multiple-particle transport in complex voxel geometries will be highly desirable because some of the most widely used Monte Carlo codes, such as the MCNP code, do not efficiently handle large amounts of voxels or moving targets. Last but not least, there will be a need to create physical phantoms to experimentally benchmark the dosimetry data obtained from tomographic models. The combination of medical imaging and 3-D rapid prototyping for computer-aided design-based phantom fabrication is an area that may deserve special attention in the future (105).

With the recent developments in radiochemistry and tracer production technology, combined with progress made in molecular/cell biology, it has become possible to design specific tracers to image events noninvasively in small animals and humans to investigate disease processes in vivo (106). The role of transgenic and knockout mice in biomedical research has now become profound and widespread, and transgenic animals (mice and rats) at this time can be designed and created in a way that offers interesting possibilities for addressing basic research questions concerning the genetic, molecular, and cellular basis of biology and disease.

While much effort has been devoted to the creation of human models, few research studies have addressed the need for models supporting small-animal imaging and dosimetry research. The recent interest in the use of mice and rats as models of human disease and related advances in molecular imaging instrumentation for biomedical research have spurred the development of realistic computerized models depicting the anatomy and physiological functions of small animals. Most previously reported small-animal models have been stylized and mathematically based (45). More recent investigations report on the development of more realistic voxel-based brain and

whole-body mouse and rat models suitable for molecular imaging research, based on actual image data obtained from serial cryo-sections (107) or using dedicated high-resolution small-animal CT scanners (108).

CONCLUSIONS

It is inspiring and gratifying to see the progress that computational anatomy modeling has made—from simple spherical geometries through stylized models of reference individuals, and most recently toward person-specific models based on patient or cadaver images. The past two decades saw exciting development efforts on tomographic human models, which were made possible by advanced medical imaging and computing technologies. To date, approximately 30 voxel-based models with unprecedented anatomical detail and realism have been painstakingly created for research in radiation dosimetry and radiological imaging, as well as in fields involving nonionizing radiation. At a voxel size of 0.33 mm $\times$ 0.33 mm $\times$ 1 mm, the VIP-Man adult male whole-body model, constructed from the color photographic images of the VHP, will remain one of the most detailed and versatile tomographic models for many years to come. VIP-Man has been adopted into state-of-the-art Monte Carlo codes, mostly for radiation transport studies and organ dose calculations. It contains small tissues, such as skin, GI track mucosa, eye lenses, and red bone marrow, that were not (or not as realistically) represented in the MIRD-based stylized models and other image-based tomographic models. Recently, respiratory motions have been added to create a 4-D VIP-Man model that can be used to study radiation treatment of lung cancer. In addition, VIP-Man has been used to study X-ray-image-quality optimization and mechanical surgical simulation. At the time this review was written, a new R01 research grant from the National Library of Medicine had been approved to develop a physics-based deformation-simulating model at Rensselaer based on the original VIP-Man platform.

These advances are significant in that we may finally create a digital human test bed for biomedical engineering research that is related not only to radiological physics principles but also to those that are biomechanical, bioelectrical, and biothermal. Such a test bed will require multiscale modeling methods that integrate organ-level data with molecular and DNA information, aided by advanced computational algorithms and cross-sectional data that do not currently exist. Research activities in tomographic modeling in the next five to ten years will be driven mostly by clinical radiological applications involving diagnostic imaging and radiotherapy, where accurate patient-specific modeling is critical. One should not be surprised if future technologies again bring opportunities for new ways of human modeling, in the same way that the 3-D imaging did to the current generation of tomographic models.

ACKNOWLEDGMENTS

H.Z. acknowledges the support of the Swiss National Science Foundation (3152A0-102143). Much of the information presented in this review about the VIP-Man model is based on research projects by formal doctoral students at Rensselaer, including

Dr. T.C. Chao, Dr. A. Bozkurt, Dr. C.Y. Shi, Dr. M. Winslow, Dr. T.T. Zhang, Dr. B. Wang, and Dr. P. Caracappa. These projects were supported by various research grants: the National Science Foundation CAREER/Biomedical Engineering Program (BES-9875532), the National Library of Medicine (1R03LM007964), and the National Cancer Institute (1R42CA115122 and 1R01CA116743). In addition, the VHP images were obtained from the National Library of Medicine.

LITERATURE CITED

1. Zaidi H. 1999. Relevance of accurate Monte Carlo modeling in nuclear medical imaging. *Med. Phys*. 26:574–608
2. Poston JW, Bolch W, Bouchet L. 2002. Mathematical models of the human anatomy. In *Therapeutic Applications of Monte Carlo Calculations in Nuclear Medicine*, ed. H Zaidi, G Sgouros, pp. 108–32. Bristol: Inst. Phys. Publ.
3. Peter J, Tornai MP, Jaszczek RJ. 2000. Analytical versus voxelized phantom representation for Monte Carlo simulation in radiological imaging. *IEEE Trans. Med. Imaging* 19:556–64
4. Goertzen AL, Beekman FJ, Cherry SR. 2002. Effect of phantom voxelization in CT simulations. *Med. Phys*. 29:492–98
5. Int. Comm. Radiol. Units Meas. 1992. Phantoms and computational models in therapy, diagnosis and protection. *ICRU Rep. 48*. Bethesda, MD: Int. Comm. Radiol. Units Meas.
6. Zaidi H, Sgouros G, eds. 2002. *Therapeutic Applications of Monte Carlo Calculations in Nuclear Medicine*. Bristol: Inst. Phys. Publ.
7. Int. Comm. Radiol. Prot. 1959. *Report of Committee II on Permissible Dose for Internal Radiation. ICRP Publication 2*. New York: Pergamon
8. Loevinger R, Budinger TF, Watson EE. 1991. *MIRD Primer for Absorbed Dose Calculations, Revised*. New York: Soc. Nucl. Med.
9. Ellet WH, Callahan AB, Brownell GL. 1964. Gamma-ray dosimetry of internal emitters. I. Monte Carlo calculations of absorbed dose from point sources. *Br. J. Radiol*. 37:45–52
10. Brownell GL, Ellet WH, Reddy AR. 1968. MIRD pamphlet no. 3: absorbed fractions for photon dosimetry. *J. Nucl. Med*. 27:27–39
11. Fisher H, Snyder W. 1966. Variation of dose delivered by 137Cs as a function of body size from infancy to adulthood. *ORNL-4007. Rep. TN 221–28*. Oak Ridge, TN: Oak Ridge Natl. Lab.
12. Snyder WS, Ford MR, Warner GG, Fisher HL. 1969. MIRD pamphlet no. 5: estimates of absorbed fractions for monoenergetic photon sources uniformly distributed in various organs of a heterogeneous phantom. *J. Nucl. Med.* 10(Suppl. 3):5–52
13. Snyder W, Ford MR, Warner G. 1978. *Estimates of Specific Absorbed Fractions for Photon Sources Uniformly Distributed in Various Organs of a Heterogeneous Phantom. Pamphlet No. 5, Revised*. New York: Soc. Nucl. Med.
14. Intl. Comm. Radiol. Prot. 1975. *Report of the Task Group on Reference Man. ICRP Publication 23*. New York: Pergamon

15. Cristy M. 1980. Mathematical phantoms representing children of various ages for use in estimates of internal dose. *Rep. ORNL/NUREG/TM-367*. Oak Ridge, TN: Oak Ridge Natl. Lab.
16. Cristy M, Eckerman KF. 1987. Specific absorbed fractions of energy at various ages from internal photon sources. *Rep. ORNL/TM 8381/V1-V7*. Oak Ridge, TN: Oak Ridge Natl. Lab.
17. Stabin MG, Watson E, Cristy M, Ryman J, Eckerman K, et al. 1995. Mathematical models and specific absorbed fractions of photon energy in the nonpregnant adult female and at the end of each trimester of pregnancy. *Rep. ORNL/TM-12907*. Oak Ridge, TN: Oak Ridge Natl. Lab.
18. Kramer R, Zankl M, Williams GGD. 1982. The calculation of dose from external photon exposures using reference human phantoms and Monte-Carlo methods, part 1: the male (ADAM) and female (EVA) adult mathematical phantoms. *Rep. GSF Bericht S-885*. Gesellschaft fur Strahlen-und Umweltforschung mbH, Munchen
19. Int. Comm. Radiol. Prot. 1996. *Conversion Coefficients for Use in Radiological Protection Against External Radiation. ICRP Publication 74*. Oxford: Pergamon
20. Bouchet LG, Bolch WE, Weber DA, Atkins HL, Poston JW. 1999. MIRD pamphlet no. 15: radionuclide S values in a revised dosimetric model of the adult head and brain. *J. Nucl. Med*. 40:S62–101
21. Bouchet LG, Bolch WE. 1999. Five pediatric head and brain mathematical models for use in internal dosimetry. *J. Nucl. Med*. 40:1327–36
22. Eckerman K, Cristy M, Warner GG. 1981. *Dosimetric evaluation of brain scanning agents.* Presented at Int. Radiopharm. Dosim. Symp., 3rd, HHS Publication FDA 81–8166, pp. 527–40. Oak Ridge, TN: U.S. Dept. Health Hum. Serv.
23. Holman BL, Zimmerman RE, Schapiro JR, Kaplan ML, Jones AG, Hill TC. 1983. Biodistribution and dosimetry of N-isopropyl-p-[123I]iodoamphetamine in the primate. *J. Nucl. Med*. 24:922–31
24. Deloar H, Watabe H, Nakamura T, Narita Y, Yamadera A, et al. 1997. Internal dose estimation including the nasal cavity and major airway for continuous inhalation of C15O2, 15O2 and C15O using the thermoluminescent dosimeter method. *J. Nucl. Med.* 38:1603–13
25. Watson EE, Stabin MG, Davis JL, Eckerman KF. 1989. A model of the peritoneal cavity for use in internal dosimetry. *J. Nucl. Med*. 30:2002–11
26. Stabin MG. 1994. A model of the prostate gland for use in internal dosimetry. *J. Nucl. Med*. 35:516–20
27. Eckerman KF, Stabin MG. 2000. Electron absorbed fractions and dose conversion factors for marrow and bone by skeletal regions. *Health Phys*. 78:199–214
28. Bouchet LG, Bolch WE, Howell RW, Rao DV. 2000. S values for radionuclides localized within the skeleton. *J. Nucl. Med*. 41:189–212
29. Poston JW, Kodimer KA, Bolch WE. 1996. A revised model for the calculation of absorbed energy in the gastrointestinal tract. *Health Phys*. 71:307–14
30. Mardirossian G, Tagesson M, Blanco P, Bouchet LG, Stabin M, et al. 1999. A new rectal model for dosimetry applications. *J. Nucl. Med.* 40:1524–31

31. Bouchet LG, Bolch WE, Blanco HP, Wessels BW, Siegel JA, et al. 2003. MIRD pamphlet no 19: absorbed fractions and radionuclide S values for six age-dependent multiregion models of the kidney. *J. Nucl. Med.* 44:1113–47
32. Siegel JA, Stabin MG. 1994. Absorbed fractions for electrons and beta particles in spheres of various sizes. *J. Nucl. Med.* 35:152–56
33. Stabin MG, Konijnenberg MW. 2000. Re-evaluation of absorbed fractions for photons and electrons in spheres of various sizes. *J. Nucl. Med.* 41:149–60
34. Clairand I, Bouchet LG, Ricard M, Durigon M, Di-Paola M, Aubert B. 2000. Improvement of internal dose calculations using mathematical models of different adult heights. *Phys. Med. Biol.* 45:2771–85
35. Huh C, Bolch WE. 2003. A review of US anthropometric reference data (1971–2000) with comparisons to both stylized and tomographic anatomic models. *Phys. Med. Biol.* 48:3411–29
36. Shepp LA, Logan BF. 1974. The Fourier reconstruction of a head phantom. *IEEE Trans. Nucl. Sci.* 21:21–43
37. Inst. Med. Phys. E. 2006. *The FORBILD phantom database*. **http://www.imp.uni-erlangen.de/phantoms/**
38. Paganetti H. 2004. Four-dimensional Monte Carlo simulation of time-dependent geometries. *Phys. Med. Biol.* 49:N75–81
39. Peter J, Gilland DR, Jaszczak RJ, Coleman RE. 1999. Four-dimensional superquadric-based cardiac phantom for Monte Carlo simulation of radiological imaging systems. *IEEE Trans. Nucl. Sci.* 46:2211–17
40. Piegl L, Tiller W. 1997. *The NURBS Book*. New York: Springer-Verlag
41. Segars WP. 2001. *Development and application of the new dynamic NURBS-based Cardiac-Torso (NCAT) phantom*. PhD thesis. Chapel Hill: Univ. North Carol. 221 pp.
42. Zhu J, Zhao S, Ye Y, Wang G. 2005. Computed tomography simulation with superquadrics. *Med. Phys.* 32:3136–43
43. Peter J, Semmler W. 2004. Integrating kinetic models for simulating tumor growth in Monte Carlo simulation of ECT systems. *IEEE Trans. Nucl. Sci.* 51:2628–33
44. LaCroix K. 1997. *Evaluation of an attenuation compensation method with respect to defect detection in Tc-99m-sestamibi myocardial SPECT*. PhD thesis. Chapel Hill: Univ. North Carol. 161 pp.
45. Segars WP, Tsui BM, Frey EC, Johnson GA, Berr SS. 2004. Development of a 4-D digital mouse phantom for molecular imaging research. *Mol. Imaging Biol.* 6:149–59
46. Bouchet LG, Bolch WE, Weber DA, Atkins HL, Poston JW. 1996. A revised dosimetric model of the adult head and brain. *J. Nucl. Med.* 37:1226–36
47. Spitzer VM, Whitlock DG. 1998. The Visible Human Dataset: the anatomical platform for human simulation. *Anat. Rec.* 253:49–57
48. Zhang SX, Heng PA, Liu ZJ, Tan LW, Qiu MG, et al. 2004. The Chinese Visible Human (CVH) datasets incorporate technical and imaging advances on earlier digital humans. *J. Anat.* 204:165–73
49. Caon M. 2004. Voxel-based computational models of real human anatomy: a review. *Radiat. Environ. Biophys.* 42:229–35

50. Kim J, Zeeberg BR, Fahey FH, Bice AN, Hoffman EJ, Reba RC. 1991. Three-dimensional SPECT simulations of a complex three-dimensional mathematical brain model and measurements of the three-dimensional physical brain phantom. *J. Nucl. Med*. 32:1923–30
51. Hoffman EJ, Cutler PD, Digby WM, Mazziotta JC. 1990. 3-D phantom to simulate cerebral blood flow and metabolic images for PET. *IEEE Trans. Nucl. Sci*. 37:616–20
52. Zubal IG, Harrell CR, Smith EO, Rattner Z, Gindi G, Hoffer BP. 1994. Computerized 3-dimensional segmented human anatomy. *Med. Phys*. 21:299–302
53. Dawson TW, Caputa K, Stuchly MA. 1997. A comparison of 60 Hz uniform magnetic and electric induction in the human body. *Phys. Med. Biol*. 42:2319–29
54. Sjogreen K, Ljungberg M, Wingardh K, Erlandsson K, Strand SE. 2001. Registration of emission and transmission whole-body scintillation-camera images. *J. Nucl. Med*. 42:1563–70
55. Kramer R, Vieira JW, Khoury HJ, Lima FR, Fuelle D. 2003. All about MAX: a male adult voxel phantom for Monte Carlo calculations in radiation protection dosimetry. *Phys. Med. Biol*. 48:1239–62
56. Kramer R, Khoury HJ, Vieira JW, Loureiro ECM, Lima VJM, et al. 2004. All about FAX: a female adult voxel phantom for Monte Carlo calculation in radiation protection dosimetry. *Phys. Med. Biol*. 49:5203–16
57. Dimbylow PJ. 1997. FDTD calculations of the whole-body averaged SAR in an anatomically realistic voxel model of the human body from 1 MHz to 1 GHz. *Phys. Med. Biol*. 42:479–90
58. Dimbylow PJ. 2002. Fine resolution calculations of SAR in the human body for frequencies up to 3 GHz. *Phys. Med. Biol*. 47:2835–46
59. Jones DG. 1997. A realistic anthropomorphic phantom for calculating organ doses arising from external photon irradiation. *Radiat. Prot. Dosim*. 72:21–29
60. Dimbylow PJ. 2005. Development of the female voxel phantom, NAOMI, and its application to calculations of induced current densities and electric fields from applied low frequency magnetic and electric fields. *Phys. Med. Biol*. 50:1047–70
61. Petoussi-Henss N, Zankl M, Fill U, Regulla D. 2002. The GSF family of voxel phantoms. *Phys. Med. Biol*. 47:89–106
62. Fill UA, Zankl M, Petoussi-Henss N, Siebert M, Regulla D. 2004. Adult female voxel models of different stature and photon conversion coefficients for radiation protection. *Health Phys*. 86:253–72
63. Zankl M, Veit R, Williams G, Schneider K, Fendel H, et al. 1988. The construction of computer tomographic phantoms and their application in radiology and radiation protection. *Radiat. Environ. Biophys*. 27:153–64
64. Caon M, Bibbo G, Pattison J. 1999. An EGS4-ready tomographic computational model of a 14-year-old female torso for calculating organ doses from CT examinations. *Phys. Med. Biol*. 44:2213–25
65. Nipper JC, Williams JL, Bolch WE. 2002. Creation of two tomographic voxel models of pediatric patients in the first year of life. *Phys. Med. Biol*. 47:3143–64
66. Lee C, Williams JL, Lee C, Bolch W. 2005. The UF series of tomographic computational phantoms of pediatric patients. *Med. Phys*. 32:3537–48

67. Nagaoka T, Watanabe S, Sakurai K, Kunieda E, Taki M, Yamanaka Y. 2004. Development of realistic high-resolution whole-body voxel models of Japanese adult males and females of average height and weight, and application of models to radio-frequency electromagnetic-field dosimetry. *Phys. Med. Biol.* 49:1–15
68. Saito K, Wittmann A, Koga S, Ida Y, Kamei T, et al. 2001. Construction of a computed tomographic phantom for a Japanese male adult and dose calculation system. *Radiat. Environ. Biophys.* 40:69–75
69. Sato K, Noguchi H, Emoto Koga Y, Saito K. 2007. Japanese adult male voxel phantom constructed on the basis of CT-images. *Radiat. Protect Dosim.* In press (doi:10.1093/rpd/ncl101)
70. Sato K, Noguchi H, Emoto Koga Y, Saito K. 2007. Construction of a Japanese adult female voxel phantom for internal dosimetry. *Radiat. Environ. Biophys.* Submitted
71. Lee C, Lee J. 2004. Korean adult male voxel model KORMAN segmented from magnetic resonance images. *Med. Phys.* 31:1017–22
72. Xu XG, Chao TC, Bozkurt A. 2000. VIP-Man: an image-based whole-body adult male model constructed from color photographs of the Visible Human Project for multi-particle Monte Carlo calculations. *Health Phys.* 78:476–86
73. Winslow M, Xu XG, Yazici B. 2005. Development of a simulator for radiographic image optimization. *Comput. Methods Programs Biomed.* 78:179–90
74. Jin W, Lim Y, Xu XG, Singh T. De S. 2005. *Improving the visual realism of virtual surgery*. Proc. Med. Meets Virtual Real. 13, pp. 227–33. Long Beach, CA: IOS Press
75. Shi CY, Xu XG. 2004. Development of a 30-week-pregnant female tomographic model from computed tomography (CT) images for Monte Carlo organ dose calculations. *Med. Phys.* 31:2491–97
76. Shi CY, Xu XG, Stabin MG. 2004. Specific absorbed fractions for internal photon emitters calculated for a tomographic model of a pregnant woman. *Health Phys.* 87:507–11
77. Zankl M, Fill U, Petoussi-Henss N, Regulla D. 2002. Organ dose conversion coefficients for external photon irradiation of male and female voxel models. *Phys. Med. Biol.* 47:2367–85
78. Int. Comm. Radiol. Prot. 2006. 2005 recommendations of the International Commission on Radiological Protection. **http://www.icrp.org/docs/Scope_of_rad_prot_draft_02_258_05v06.pdf**
79. Kramer R, Khoury HJ, Vieira JW, Lima VJM. 2006. MAX06 and FAX06: update of two adult human phantoms for radiation protection dosimetry. *Phys. Med. Biol.* 51:3331–46
80. Ferrari P, Gualdrini G. 2005. An improved MCNP version of the NORMAN voxel phantom for dosimetry studies. *Phys. Med. Biol.* 50:4299–316
81. Lee C, Lee C, Park SH, Lee JK. 2006. Development of the two Korean adult tomographic computational phantoms for organ dosimetry. *Med. Phys.* 33:380–90
82. Beddoe A. 1976. *The microstructure of mammalian bone in relation to the dosimetry of bone-seeking radionuclides*. Leeds: Univ. Leeds

83. Int. Comm. Radiol. Prot. 1995. *Basic Anatomical and Physiological Data for Use in Radiological Protection: The Skeleton*. *ICRP Publication 70*. Oxford: Pergamon
84. Caracappa P, Xu X. 2006. A revised method of estimating red bone marrow dose in image-based computational models. *Health Phys.* 90:S122 (Abstr.)
85. Bolch WE, Patton PW, Rajon DA, Shah AP, Jokisch DW, Inglis BA. 2002. Considerations of marrow cellularity in 3-dimensional dosimetric models of the trabecular skeleton. *J. Nucl. Med*. 43:97–108
86. Int. Comm. Radiol. Prot. 2002. *Annual report of the ICRP*. **http://www.icrp.org/docs/2002_Ann_Rep_52_429_03.pdf**
87. Int. Comm. Radiol. Prot. 2002. Basic anatomical and physiological data for use in radiological protection: reference values. ICRP publication 89. *Ann. ICRP* 32:1–277
88. Ponisch F, Parodi K, Hasch BG, Enghardt W. 2004. The modelling of positron emitter production and PET imaging during carbon ion therapy. *Phys. Med. Biol.* 49:5217–32
89. Lazaro D, El Bitar Z, Breton V, Hill D, Buvat I. 2005. Fully 3D Monte Carlo reconstruction in SPECT: a feasibility study. *Phys. Med. Biol*. 16:3739–54
90. Soares EJ, Glick SJ, Hoppin JW. 2005. Noise characterization of block-iterative reconstruction algorithms: II. Monte Carlo simulations. *IEEE Trans. Med. Imaging* 24:112–21
91. Zaidi H, Koral KF. 2004. Scatter modelling and compensation in emission tomography. *Eur. J. Nucl. Med. Mol. Imaging* 31:761–82
92. Gustafsson A, Bake B, Jacobsson L, Johansson A, Ljungberg M, Moonen M. 1998. Evaluation of attenuation corrections using Monte Carlo simulated lung SPECT. *Phys. Med. Biol*. 43:2325–36
93. Arlig A, Gustafsson A, Jacobsson L, Ljungberg M, Wikkelso C. 2000. Attenuation correction in quantitative SPECT of cerebral blood flow: a Monte Carlo study. *Phys. Med. Biol*. 45:3847–59
94. Zaidi H, Montandon ML, Slosman DO. 2004. Attenuation compensation in cerebral 3D PET: effect of the attenuation map on absolute and relative quantitation. *Eur. J. Nucl. Med. Mol. Imaging* 31:52–63
95. Dewaraja YK, Ljungberg M, Koral KF. 2001. Monte Carlo evaluation of object shape effects in iodine-131 SPET tumor activity quantification. *Eur. J. Nucl. Med*. 28:900–6
96. Frouin V, Comtat C, Reilhac A, Gregoire MC. 2002. Correction of partial volume effect for PET striatal imaging: fast implementation and study of robustness. *J. Nucl. Med*. 43:1715–26
97. Zaidi H, Scheurer AH, Morel C. 1999. An object-oriented Monte Carlo simulator for 3D cylindrical positron tomographs. *Comput. Methods Programs Biomed*. 58:133–45
98. Zaidi H. 2000. Object-oriented programming environments: a promising tool for biomedical imaging research. *Pol. J. Med. Phys. Eng*. 6:71–89
99. Zaidi H, Labbé C, Morel C. 1998. Implementation of an environment for Monte Carlo simulation of fully 3D positron tomography on a high-performance parallel platform. *Parallel Comput*. 24:1523–36

100. Ay M, Zaidi H. 2005. Development and validation of MCNP4C-based Monte Carlo simulator for fan- and cone-beam X-ray CT. *Phys. Med. Biol*. 50:4863–85
101. Ay M, Shahriari M, Sarkar S, Adib M, Zaidi H. 2004. Monte Carlo simulation of X-ray spectra in diagnostic radiology and mammography using MCNP4C. *Phys. Med. Biol*. 49:4897–917
102. Ay M, Zaidi H. 2006. Assessment of errors caused by X-ray scatter and use of contrast medium when using CT-based attenuation correction in PET. *Eur. J. Nucl. Med. Mol. Imaging* 33:1301–13
103. Xu XG, Shi C. 2005. *Preliminary development of a 4D anatomical model for Monte Carlo simulations*. Presented at Proc. Monte Carlo Method: Versatility Unbounded Dyn. Comput. World, Chattanooga, Tenn.
104. Xu XG, Chao TC, Bozkurt A. 2005. Comparison of effective doses from various monoenergetic particles based on the stylised and the VIP-Man tomographic models. *Radiat. Prot. Dosim*. 115:530–35
105. Xu XG, Hanlon J, Oakley M. 2006. *A feasibility study to fabricate a lung phantom from medical images and computer aided manufacturing*. Proc. Am. Nucl. Soc. Bienn. Top. Meet. Radiat. Prot. Shield. Div., 14th, pp. 183–85, Carlsbad, NM
106. Cherry SR. 2004. In vivo molecular and genomic imaging: new challenges for imaging physics. *Phys. Med. Biol.* 49:R13–48
107. Beekman FJ, Vastenhouw B. 2004. Design and simulation of a high-resolution stationary SPECT system for small animals. *Phys. Med. Biol*. 49:4579–92
108. Stabin MG, Peterson TE, Holburn GE, Emmons MA. 2006. Voxel-based mouse and rat models for internal dose calculations. *J. Nucl. Med*. 47:655–59
109. Petoussi-Henss N, Zankl M. 1998. Voxel anthropomorphic models as a tool for internal dosimetry. *Radiat. Prot. Dosim*. 79:415–18
110. Zankl M, Wittmann A. 2001. The adult male voxel model "Golem" segmented from whole-body CT patient data. *Radiat. Environ. Biophys*. 40:153–62